Title

Improvement of Oxidation Resistance for Ni-base Single Crystal Superalloy TMS-238 by Suppression of Sb Segregation at Oxide/Substrate Interface Using CaO

Authors

HIROTOSHI MAEZAWA[1,2], CHIHIRO TABATA[2,3], YUJI TAKATA[2], JUN UZUHASHI[2], TADAKATSU OHKUBO[2], TADAHARU YOKOKAWA[2], HIROSHI HARADA[2], KYOKO KAWAGISHI[2,3], and SHINSUKE SUZUKI[1,3,4]

Affiliations

1 Department of Applied Mechanics and Aerospace Engineering, Waseda University: 3-4-1 Okubo, Shinjuku, Tokyo, 169-8555, Japan

2 National Institute for Materials Science (NIMS): 1-2-1 Sengen, Tsukuba, Ibaraki, 305-0047, Japan

3 Department of Materials Science, Waseda University: 3-4-1 Okubo, Shinjuku, Tokyo, 169-8555, Japan

4 Kagami Memorial Institute for Materials Science and Technology, Waseda University: 2-8-26 Nishiwaseda, Shinjuku, Tokyo, 169-0051, Japan

HIROSHI HARADA is now with Superalloy Design Laboratory, 3-18-33, Azuma, Tsukuba, Ibaraki, 305-0031, Japan.

Corresponding Author

HIROTOSHI MAEZAWA, hirowolves5@suou.waseda.jp

Abstract

Impurity Sb degrades the oxidation resistance of Ni-base superalloys after Al_2O_3 crucible melting. The purpose of this study is to clarify the effect of CaO on the oxidation resistance of Ni-base single crystal superalloy TMS-238 containing Sb and the reaction mechanism. Single crystal alloys containing Sb were cast using an Al_2O_3 crucible and a CaO crucible. In the cyclic oxidation tests, the mass did not decrease for the alloy after CaO crucible melting. In STEM observations for the alloy after CaO crucible melting, Sb-Ca-O inclusion was found. In 3DAP for the oxide/substrate interface of the alloy after CaO crucible melting, Sb segregation was not detected. Moreover, the CaO rod was inserted in the TMS-238 melt to observe the CaO/melt interface. In EPMA observations of the surface of the CaO rod, Sb was observed. Therefore, the higher oxidation resistance of the alloy after CaO crucible melting than that of Al_2O_3 crucible melting is due to the suppression of Sb segregation at the oxide/substrate interface by removing Sb from the melt and fixing Sb in the alloy. These occur by the formation of Sb-Ca-O on the surface of CaO, and the formation of Sb-Ca-O inclusions in the alloy, respectively.

I. INTRODUCTION

Ni-base superalloys are used in turbine blades for jet engines and gas turbines for power generation because of their superior high-temperature properties. To improve the thermal efficiency of jet engines and gas turbines for power generation, it is necessary to increase the turbine inlet temperature. For this reason, rare metals such as Re, Ta, W, and Ru are added to Ni-base superalloys to improve their high-temperature properties.[1–5] Our research group developed the 6th generation Ni-base single crystal (SC) superalloy TMS-238, which has the highest temperature capability in history.[1] However, an increase in material cost due to the addition of rare metals is an issue. Therefore, our research group has been studying the "direct and complete recycling method", where used turbine blades are directly melted and recast to produce recycled materials.[6,7] This leads to the possibility of using various low-purity materials to reduce the cost of ingots production. However, low-purity materials contain impurities.[8–10] Takata *et al.* revealed that low melting point metallic impurity Sb significantly degrades the oxidation resistance of Ni-base SC superalloy TMS-238, and it was assumed that Sb segregated at the oxide/substrate interface, leading to the acceleration of the spallation of the oxide layers and degradation of the oxidation resistance.[11] To improve the oxidation resistance of Ni-base SC superalloy containing Sb, it is necessary to suppress Sb segregation at the oxide/substrate interface by removing Sb from the melt or fixing Sb in the alloy.

Regarding the removal of impurities from the melt, it was found that about 90 pct of Sb can be removed from Ni-base alloy NCF-1 (14/17Cr-6/10Fe-Ni) by MSR (Metal bearing Solution Refining) using 6 pct Ca-CaF_2 flux.[12] However, the use of CaF_2 has been reduced due to environmental

concerns.[13] It was also found that about 40 pct of Sb can be removed from crude copper as Sb oxides by using CaO-Na_2SO_4 flux.[14] Our research group reported the effect on removing impurity S by contacting CaO with Ni-base superalloy melts. The reaction of Al in the melt with CaO forms calcium aluminate and Ca. It was revealed that S is removed by CaS incorporated into calcium aluminate.[15,16]

Regarding the fixation of an impurity in the alloy, CaO crucible melting for the Ni-base superalloy is effective for fixing impurity S in the alloy. Ca dissolves into the melt by the reaction of Al and CaO in the molten metal, and S is fixed in the alloy by the formation of CaS inclusions. This suppresses S segregation at the oxide/substrate interface and suppresses the spallation of the oxide layers, thereby improving the oxidation resistance.[17,18]

Based on these previous studies, it can be hypothesized that impurity Sb can be removed from the melt and fixed in the alloy as inclusions by using CaO, which can improve the oxidation resistance of the alloys. However, the effect of CaO on the oxidation resistance of Ni-base SC superalloys containing Sb has not been clarified.

The purpose of this study is to clarify the effect of CaO on the oxidation resistance of Ni-base SC superalloys TMS-238 containing Sb and the reaction mechanism. The recycling of TMS-238, which contains many rare metals, is beneficial for the use spread of the highest temperature capable superalloy. Cyclic oxidation tests were conducted to reveal whether the oxidation resistance had improved by using the CaO crucible, and microstructures were investigated to reveal whether Sb segregation at the oxide/substrate interface had been suppressed and if Sb inclusions had formed in the alloy. In addition, a CaO rod was inserted into TMS-238 melt, and the CaO rod was analyzed to observe the reaction at the CaO/melt interface to reveal whether Sb had been removed from the melt, and the mechanism was discussed.

II. EXPERIMENTAL PROCEDURES

A. *Evaluation of Oxidation Resistance and Microstructure Investigation of Alloys*

An ingot of Ni-base single crystal superalloy TMS-238[1] (IHI Master Metal Co., Ltd.) was used in this study. Three types of alloys were fabricated in this study: the alloy without Sb addition that was melted in an Al_2O_3 crucible is called TMS-238(Al_2O_3), the alloy with Sb addition that was melted in an Al_2O_3 crucible is called TMS-238+Sb(Al_2O_3), and the alloy with Sb addition that was melted in a CaO crucible is called TMS-238+Sb(CaO).

A 2 kg ingot was placed in an Al_2O_3 crucible or a CaO crucible and heated at 1600 °C using high frequency vacuum heating. The pressure within the furnace was kept under 6×10^{-2} Pa. A Ni tube filled with a bulk of 10 ppm of Sb was added to the melt for TMS-238+Sb(Al_2O_3) and TMS-238+Sb(CaO). The melt was poured into a ZrO_2-base mold with a starter and a selector held at

1500 °C. Single crystal round bars (diameter: 11 mm, length: 135 mm) were cast by withdrawing the mold from the heating chamber to the cooling chamber at 200 mm/h.

The alloys were solution heat treated at 1335 °C for 20 h, aging heat treated at 1150 °C for 2 h, and secondary aging heat treated at 870 °C for 20 h.

The chemical compositions for each alloy were analyzed using inductivity-coupled plasma optical emission spectrometer (ICP-OES) (Agilent, 720-ES). For ICP-OES, 10 specimens with 0.5 mm in thickness were cut out from the starters of each alloy. The concentrations of trace elements Sb, Ca, and S were measured for each alloy using glow discharge mass spectrometry (GD-MS) (Thermo Scientific, VG9000). For GD-MS, a specimen with 5 mm in height was cut out from the starters of each alloy.

Cyclic oxidation tests were performed as follows. Round bars of each alloy were cut into cylindrical specimens (diameter: 9 mm, height: 5 mm) and the surfaces of the specimens were ground with SiC P600 and washed with acetone. Cyclic oxidation tests at 1100 °C for 1 h and air-cooling for 1 h in laboratory air were performed on all specimens. This process was repeated for 200 cycles, and the change in mass was measured after several cycles.

Microstructures were investigated by using scanning electron microscopy (SEM), 3D atom probe (3DAP), and scanning transmission electron microscopy (STEM) techniques. A needle-shaped specimen for 3DAP was prepared using focused ion beam (FIB)-SEM dual-beam system (FEI, Helios G4UX) from the TMS-238+Sb(CaO) performed the oxidation test at 1100 °C for 1 h. The elemental distribution at the oxide/substrate interface was measured using 3DAP (CAMECA, LEAP5000XS). Circular backscattered (CBS)-SEM observations of the starter of TMS-238+Sb(CaO) before heat treatment were performed, and a thin foil specimen was also prepared using FIB-SEM. The STEM system with energy-dispersive X-ray spectroscopy (EDS) (FEI, Titan G2 80-200 ChemiSTEM) was used to obtain high-angle annular dark-field (HAADF)-STEM images, EDS elemental maps, and nano-beam electron diffraction (NBED) analysis.

B. *Evaluation of Reaction at CaO/Melt Interface by Inserting CaO Rod in Melt*

CaO rod insertion experiments were performed using the high frequency vacuum heating furnace in Figure 1 as follows. Similar experiments previously performed for removal of S from Ni-base superalloy melt.[15,16] Dense CaO rods (diameter: 15 mm, length: 80 mm, porosity: <1 pct) were used to observe the reaction at the CaO/melt interface. Ingots of TMS-238 and pure Ni (Nilaco Co.) were used to compare the reaction depending on the different amounts of Al in the melt. Additive Sb was prepared by filling a Ni tube with a bulk of Sb equal to 100 ppm of the weight of the alloys.

A 500 g ingot was placed in an Al_2O_3 crucible and melted in the high frequency vacuum heating furnace. The pressure in the furnace was adjusted to less than 50 Pa at the start of heating (Figure 2(a)). The furnace was preset so that the melt heated up to 1500 °C after 56 min from the start of

heating. The CaO rod was preheated by suspending above the melt with a 40 mm gap between the bottom surface and the melt (Figure 2(b)). Sb was added by putting the Ni tube containing Sb into the melt at exactly 65 min from the start of heating (Figure 2(c)). The melt was heated up to 1600 °C within 1 min from the addition of Sb (Figure 2(d,e)). This temperature was kept throughout the rest of the experiment. 66 min from the start of heating is defined as the holding time t=0 s. In the experiments using TMS-238, two types of experiments were carried out in which heating was stopped at t=0 and 240 s. The reason why heating was stopped at t=0 s is that Sb may evaporate from the melt and be deposited on the CaO rod before being inserted into the melt, and the CaO rod before being inserted into the melt needed to be analyzed to distinguish Sb reacted in the melt from Sb deposited by evaporation. In the experiment using pure Ni, one type of experiment was carried out in which the heating was stopped at t=240 s. These experiments will be referred to as 0s(TMS-238), 240s(TMS-238), and 240s(pure Ni), respectively. In the experiment of 0s(TMS-238), the CaO rod was pulled up from the preheating position when the heating was stopped at t=0 s (Figure 2(d)). In the experiments of 240s(TMS-238) and 240s(pure Ni), the CaO rod was inserted into the melt, and the length of the rod below the surface of the melt was 35 mm at t=0 s (Figure 2(e)). The CaO rod was kept in the melt and pulled out from it when the heating was stopped at t=240 s (Figure 2(f)).

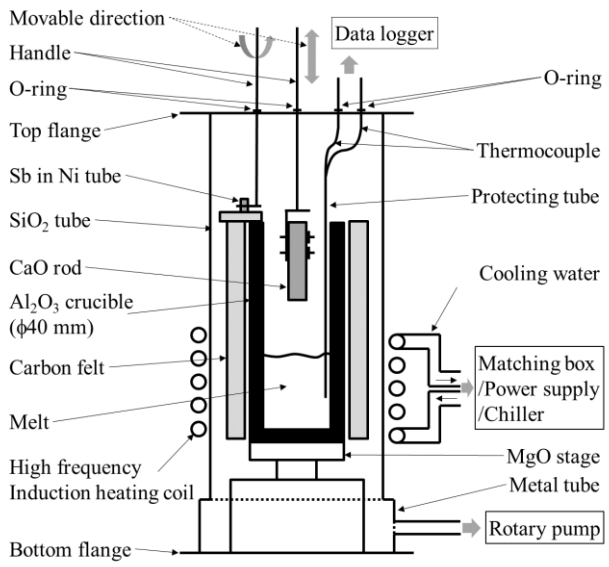

Fig. 1—Schematic diagram of the high frequency vacuum heating furnace for the CaO rod insertion experiments (adapted from the reference[16]). Some parts were modified for the experiments in this study.

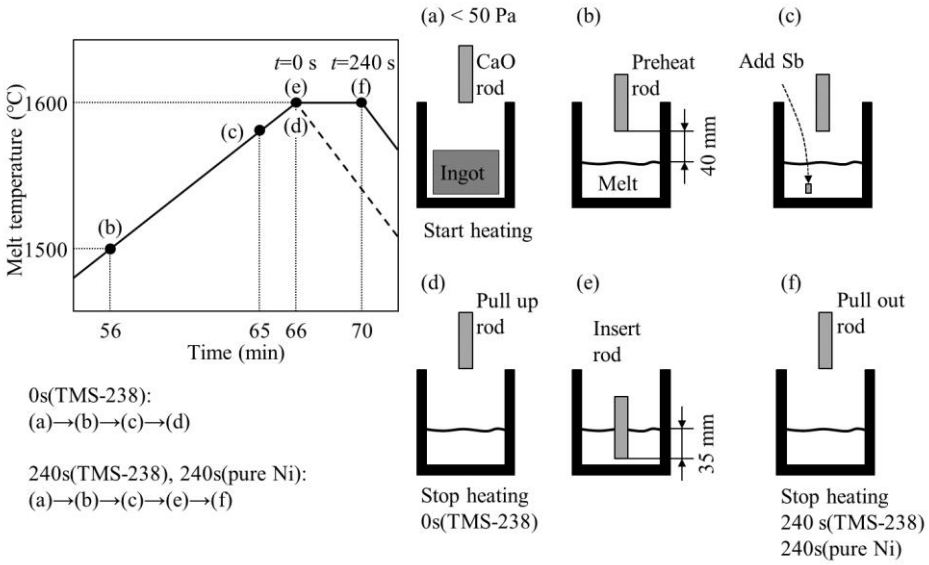

Fig. 2—Flow and schematic diagrams of the CaO rod insertion experiments. (a) Start of heating ingot, (b) preheating CaO rod, (c) adding Sb, (d) pulling up CaO rod from preheating position and finish of heating (0s(TMS-238)), (e) inserting CaO rod, and (f) pulling out CaO rod from melt and finish of heating (240s(TMS-238) and 240s(pure Ni)).

After the CaO rod insertion experiments, two sector-shaped specimens were cut out from the upper, middle, and lower parts of the alloys, respectively, as shown in Figure 3(a). These specimens were dissolved in hydrofluoric acid and nitric acid, and the elemental concentrations in the alloys were measured. The concentrations of Ni, Co, Cr, Mo, W, Al, Ta, Hf, Re, and Ru in TMS-238 and Al in pure Ni were measured using ICP-OES (Agilent, 720-ES) and the concentrations of Sb were measured using inductivity-coupled plasma mass spectrometer (ICP-MS) (Agilent, 7700).

CaO rods used in the experiments were analyzed using electron probe micro analyzer (EPMA) (Shimadzu Co., EPMA-1610) and x-ray photoelectron spectroscopy (XPS) (JEOL Ltd., JPS-9010). As shown in Figure 3(b), CaO rods were cut 5 mm from the bottom, filled with resin, and polished. Backscatter electron (BSE) images and elemental maps at the interface between the CaO rod and resin were obtained. Spectra for the binding energy of the bottom surface of the CaO rod were also obtained.

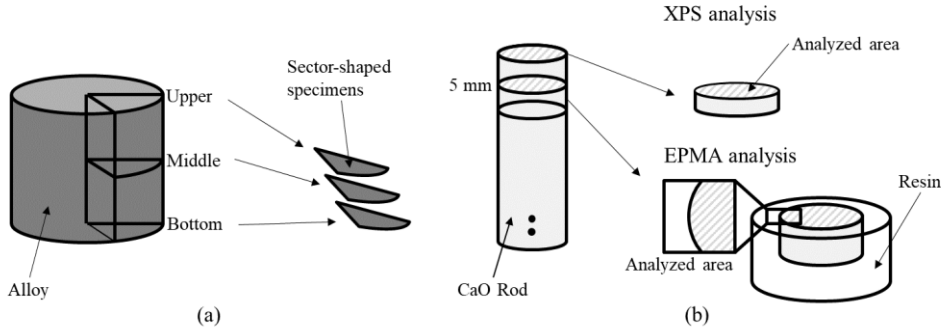

Fig. 3—Schematic diagram of the specimen preparation. (a) Specimens for ICP-OES and ICP-MS of the alloys after CaO rod insertion experiments and (b) specimens for EPMA and XPS analyses of the CaO rods.

III. RESULTS

A. *Evaluation of Oxidation Resistance and Microstructure Investigation of Alloys*

Table I shows the nominal composition of TMS-238[1] and the chemical compositions of the samples prepared for this study. Sb concentrations in both TMS-238+Sb(Al_2O_3) and TMS-238+Sb(CaO) were higher than that in TMS-238(Al_2O_3), and Ca concentration was high in TMS-238+Sb(CaO). In GD-MS, 1 ppm was the smallest order of magnitude in this study. Therefore, note that S contents were similar in all alloys.

Table I. Chemical compositions of the alloys (Ni bal.)[1]

Sample	wt pct									ppm		
	Co	Cr	Mo	W	Al	Ta	Hf	Re	Ru	Sb	Ca	S
TMS-238 (nominal)	6.5	4.6	1.1	4.0	5.9	7.6	0.1	6.4	5.0	-	-	-
TMS-238 (Al_2O_3)	6.3	4.4	1.1	4.0	5.8	7.7	0.10	6.4	5.0	0.11	<0.1	1.9
TMS-238 +Sb(Al_2O_3)	6.5	4.5	1.1	4.1	6.1	7.9	0.12	6.4	5.0	8.1	0.02	2.1
TMS-238 +Sb(CaO)	6.5	4.5	1.1	4.1	6.0	7.9	0.11	6.4	5.0	9.5	5.5	1.0

Figure 4 shows the results of the cyclic oxidation test. There was no obvious difference in the initial oxidation for all alloys. However, after 50 cycles, as the number of cycles increased, the masses of TMS-238(Al_2O_3) and TMS-238+Sb(Al_2O_3) decreased. The loss of mass for TMS-238+Sb(Al_2O_3)

was larger than that for TMS-238(Al_2O_3), which was also seen in the study by Takata *et al.*[11]. Remarkably, the mass did not decrease for TMS-238+Sb(CaO).

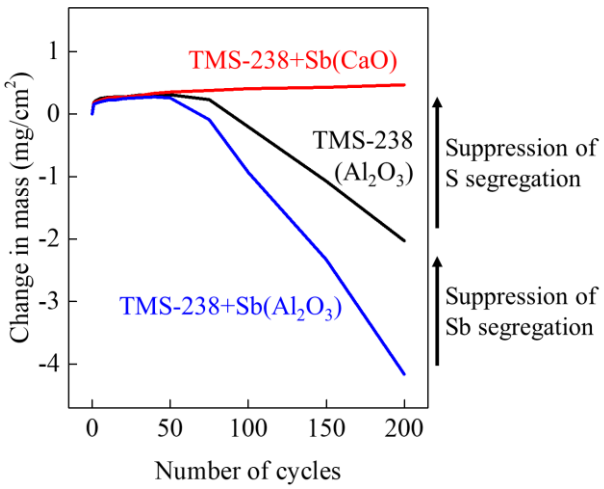

Fig. 4—Results of the cyclic oxidation tests of TMS-238(Al_2O_3), TMS-238(Al_2O_3), and TMS-238+Sb(CaO) for 200 cycles at 1100 °C in laboratory air.

Figure 5 shows the result of 3DAP of the oxide/substrate interface of TMS-238+Sb(CaO) after an oxidation test at 1100 °C for 1 h. Figure 5(a) shows the 3D atom map. The alloy containing Ni and Al, and the oxide layers containing Al and O were measured. The concentration of S was also measured to take the influence of both Sb and S segregation at the oxide/substrate interface on the oxidation resistance into account. Figure 5(b) shows the concentration profiles of Ni, Al, O, and 34 Da, which were drawn under the same condition as the study by Tabata *et al.*[17]. The reason why the peak at 34 Da shows the S concentration is described in Tabata *et al.*[17]. The amount of S segregation was almost equal to that of the alloy melted in the CaO crucible shown in the study by Tabata *et al.*[17]. Figure 5(c,d) shows the mass spectrum. Peaks at 60.45 Da, 61.45 Da, 120.9 Da, and 122.9 Da, which indicate $^{121}Sb^{++}$, $^{123}Sb^{++}$, $^{121}Sb^{+}$, and $^{123}Sb^{+}$, could not be recognized in the spectrum. Generally, the chemical sensitivity of 3DAP technique is a few per a million atoms.[19] Thus, it is concluded that there is no detectable Sb segregation at the oxide/substrate interface of TMS-238+Sb(CaO) by 3DAP method.

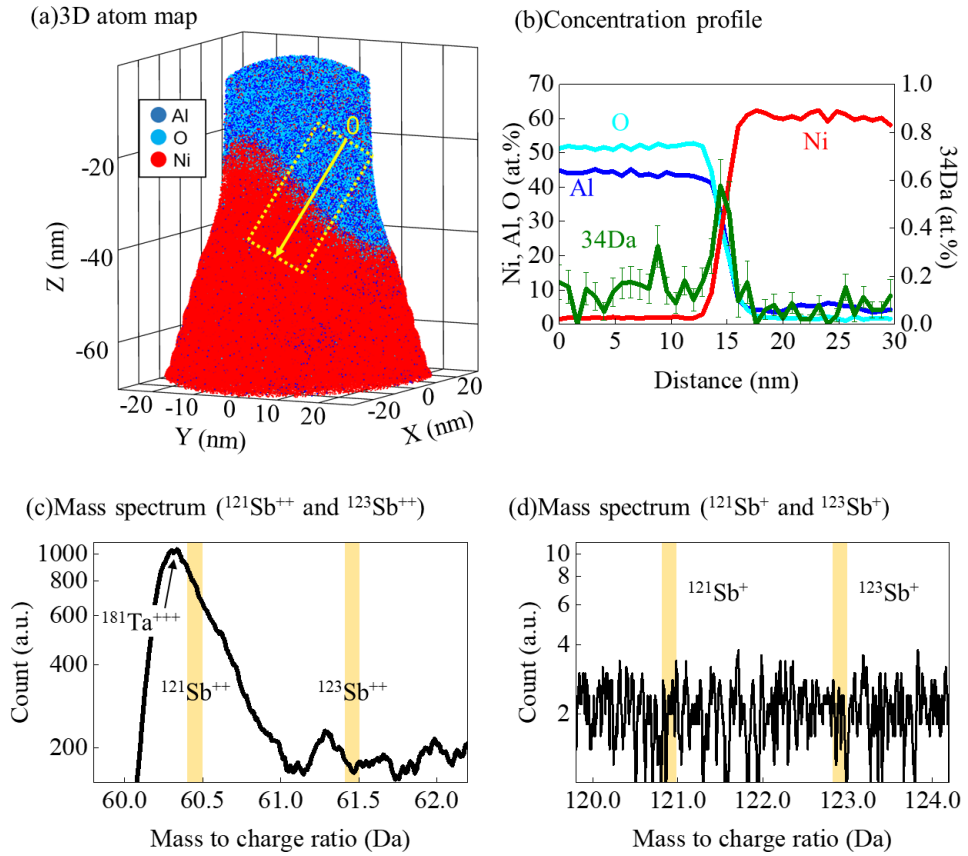

Fig. 5—Results of 3DAP for TMS-238+Sb(CaO) oxidized at 1100℃ for 1 h. (a) 3D atom map, (b) concentration profiles of Ni, Al, O, and 34 Da with standard deviation (the yellow region on (a) represents the area analyzed to obtain (b)) , (c) mass spectrum ($^{121}Sb^{++}$ and $^{123}Sb^{++}$, 60.0 to 62.0 Da), and (d) mass spectrum ($^{121}Sb^{+}$ and $^{123}Sb^{+}$, 120.0 to 124.0 Da).

FIB-SEM and STEM observations were performed to confirm the formation of Sb inclusions in the alloy by CaO crucible melting. Figure 6 shows the results for the starter of TMS-238+Sb(CaO) before heat treatment. Figure 6(a) shows the CBS-SEM image, and the inclusion, which looks black when observed using SEM, was found near the grain boundary and contained Sb with EDS attached to the FIB system. Note that inclusions that look white contained Re etc. and are likely not to affect the fixation of Sb in the alloy. The inclusion, which looks black when observed using SEM, near the grain boundary was lifted out and thinned to the TEM specimen using the FIB-SEM system. Figure 6(b) shows the cross-sectional HAADF-STEM image of the inclusion. Note that the surfaces of the inclusion and the alloy were capped with Pt as protection against FIB damage. The center of the inclusion (the darkest contrast) was confirmed to be a void. Figure 6(c) shows the STEM-EDS maps shown by at pct. Sb, Ca, Zr, and O were found in the inclusion. Figure 6(d) shows the structure of the inclusion was determined by using NBED technique and the NBED pattern. The pattern shows

the halo ring, indicating that the inclusion is amorphous.

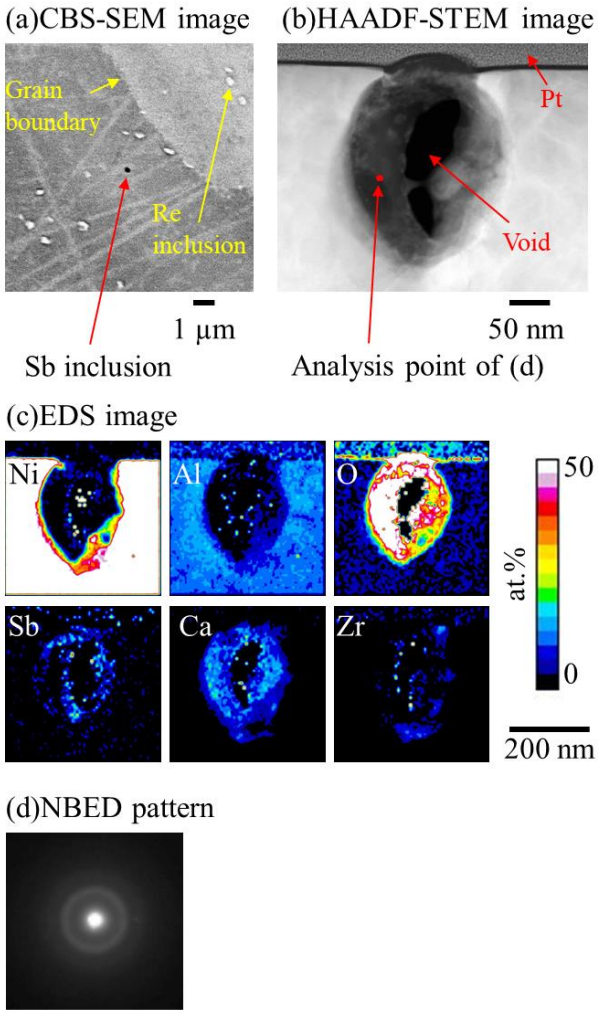

Fig. 6—Results of FIB-SEM and STEM observations for the starter of TMS-238+Sb(CaO) before heat treatment. (a) CBS-SEM image, (b) HAADF-STEM image, (c) STEM-EDS maps, and (d) NBED pattern. The plot on (b) represents the point analyzed to obtain (d).

B. *Evaluation of Reaction at CaO/Melt Interface by Inserting CaO Rod in Melt*

Table II shows the Sb contents in the alloys of 0s(TMS-238), 240s(TMS-238), and 0s(pure Ni) obtained by ICP-MS. Moreover, Table III shows the composition of 240s(TMS-238) and Al content in the alloy of 0s(pure Ni) obtained by ICP-OES. There was no significant difference between the nominal composition of TMS-238 and the chemical composition of the alloy of 240s(TMS-238). The alloy of 240s(pure Ni) contains Al.

Table II. Sb contents in the alloys (ppm)

Sample	Sb
0s(TMS-238)	93.7
240s(TMS-238)	107.4
240s(pure Ni)	69.6

Table III. Chemical compositions of the alloys (Ni bal., wt pct)

Sample	Co	Cr	Mo	W	Al	Ta	Hf	Re	Ru
240s(TMS-238)	4.4	4.5	1.1	4.1	5.9	7.7	0.11	6.9	5.0
240s(pure Ni)	-	-	-	-	0.025	-	-	-	-

Figure 7 shows the results of EPMA analysis for the CaO rods. For 240s(TMS-238), Al was detected on the surface and in the particle boundaries of the CaO rod. For 240s(pure Ni), Al was detected in the particle boundaries of the CaO rod. The particle boundaries were formed because the CaO rods was made by sintering CaO particles. The results for Sb are after interference corrections. The interference correction method applied in this study is described in Appendix. Sb was detected on the surface of the CaO rods of 240s(TMS-238) and 0s(TMS-238). The Sb concentration for 240s(TMS-238) was higher than that of 0s(TMS-238).

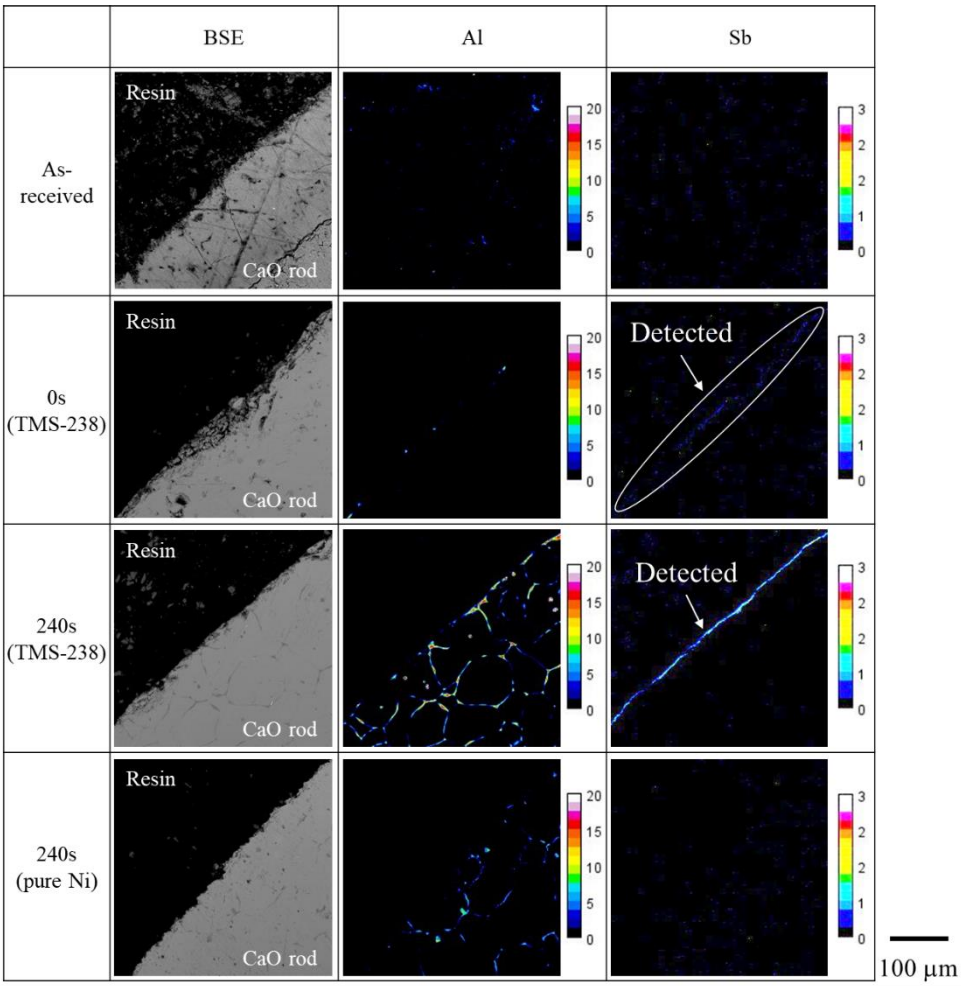

Fig. 7—Results of EPMA analysis for the CaO rods. BSE images and elemental maps showing the distributions of Al and Sb (after interference correction, explained in Appendix). The unit of the color bars is wt pct.

Figure 8 shows the results of XPS analysis of the CaO rods before and after the CaO rod insertion experiment. The dotted red line shows the peak position of Sb_2O_3[20], and the single-dashed blue line shows the peak position of Sb[21]. Neither Sb nor Sb_2O_3 peaks were observed for the as-received CaO rod and the CaO rod of 240s(pure Ni). On the other hand, the Sb_2O_3 peak was observed for the CaO rods of 0s(TMS-238) and 240s(TMS-238).

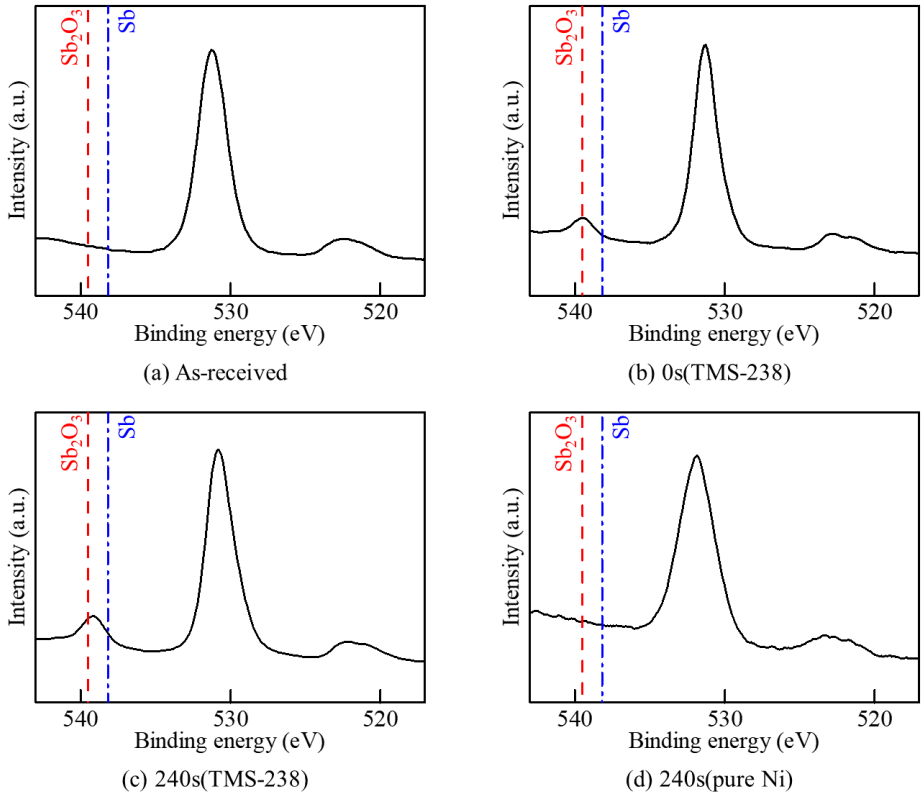

Fig. 8—Results of XPS analysis of the CaO rods. (a) As-received, (b) 0s(TMS-238), (c) 240s(TMS-238), and (d) 240s(pure Ni). The dotted line shows the peak position of Sb_2O_3[20], and the single-dashed line shows the peak position of Sb[21].

IV. DISCUSSION

A. *Effect on Improvement of Oxidation Resistance*

The effect on the improvement of oxidation resistance by CaO crucible melting is discussed here. In the cyclic oxidation tests shown in Figure 4, TMS-238+Sb(Al_2O_3) showed the largest weight loss, while TMS-238+Sb(CaO) had little change in the mass, indicating that CaO crucible melting improved the oxidation resistance for Ni-base superalloy containing impurity Sb. Because there is no obvious difference in the initial oxidation of all samples, the difference in weight loss is considered to be the difference in the amount of spallation of the oxide layers. Takata *et al.* reported that the oxidation resistance of Ni-base superalloy containing Sb after Al_2O_3 crucible melting had significantly degraded and Sb segregated at the oxide/substrate interface.[11] Takata *et al.* reported that 1.1 ppm of Sb had a negative effect on the oxidation resistance of the alloy, and when the Sb content was at 3.8 ppm, Sb segregation was observed. The Sb concentration is about 0.15 at pct at

oxide/substrate interface. In this study, the amount of Sb in the alloy melt using a CaO crucible was 9.5 ppm, which is significantly larger than the Sb-containing alloy melt using an Al_2O_3 crucible in the previous study[11]. However, for the sample melt using a CaO crucible, the Sb peak was not detected at the oxide/substrate interface in the mass spectrums from Figure 5(c). Therefore, Sb segregation at oxide/substrate interface is considered to have facilitated a spallation of oxide layers in the samples melted in an Al_2O_3 crucible. Thus, it is thought that CaO crucible melting suppressed Sb segregation at the oxide/substrate interface, resulting in the prevention of spallation of the oxide layers and the improvement of oxidation resistance.

It should also be noted that S segregated at the oxide/substrate interface as the concentration profiles shown in Figure 5(b). However, the amount of S segregation at the oxide/substrate interface was thought to have been reduced by CaO crucible melting as reported in the study by Tabata *et al.*[17]. If CaO only had an effect on Sb segregation, it would be expected that oxidation resistance would recover from TMS-238+Sb(Al_2O_3) to TMS-238(Al_2O_3) because S segregation would still remain. However, the oxidation resistance improved from TMS-238+Sb(Al2O3) to TMS-238+Sb(CaO) by using CaO in this study. Therefore, CaO crucible melting suppressed both S and Sb segregations at the oxide/substrate interface of the Sb-containing alloy. When only the suppression of Sb segregation is considered, it is thought that the oxidation resistance of the Sb-containing alloy improved to the same level or more than that of the Sb-free alloy at least. In addition, the suppression of S segregation is considered, it is thought that the oxidation resistance of the Sb-containing alloy improved to the same level of the Sb-free alloy melted in a CaO crucible.

B. *Reaction at CaO/Melt Interface*

The process of Ca formation contributing to the formation of inclusions is discussed here. Ca and Al were detected in the CaO rod of 240s(TMS-238) as the elemental maps of CaO rods shown in Figure 7 and Ca was detected in TMS-238+Sb(CaO) as the results of GD-MS for the alloys shown in Table I. These results suggest that, as reported in the previous studies[16,18,22,23], the following reaction occurred, in which Al in the melt reacted with CaO to form calcium aluminate and Ca. Through this reaction, Ca dissolved into the melt.

$$3CaO + 2Al = 3Ca + Al_2O_3 \#[1]$$

$$CaO + Al_2O_3 = CaAl_2O_4 \#\#[2]$$

Next, the reaction and the effect on removing Sb are discussed. As shown in Figure 7, Sb was not detected in the as-received CaO rod but concentrated on the surface of the CaO rod of 0s(TMS-238), indicating that Sb evaporated from the melt, and the deposit may have been observed on the surface of the CaO rod before inserting. Moreover, Sb concentrated on the surface of the CaO rod of

240s(TMS-238), with a higher Sb concentration than that of 0s(TMS-238). Therefore, CaO has the effect on removing Sb from Ni-base superalloy melt. However, the free surface area of the melt was large relative to the volume of the melt, resulting in a large amount of Sb evaporation. Therefore, it was not possible to distinguish the amount of Sb removal by CaO and the amount of Sb evaporation. Here, the removal reaction of Sb at the CaO/melt interface is discussed. Sb was not observed on the CaO rod of 240s(pure Ni). Al was also detected in the particle boundaries of the CaO rod of 240s(pure Ni). The alloy of 240s(pure Ni) contained small amounts of Al as shown in Table III. It is considered that the Al entered the melt from the Al_2O_3 crucible and entered the particle boundaries of the CaO rod but was not enriched on the surface of the CaO rod. Therefore, the reaction of Eq. [1] did not occur on the surface of the CaO rod. On the other hand, the inclusion in the alloy after CaO crucible melting consists of Sb, Ca, O, etc., and Al did not concentrate in the inclusion as shown in Figure 6. These results suggest that the removal reaction of Sb at the CaO/melt interface requires simple substance Ca, which is formed on the surface of the CaO rod by the reaction between CaO and Al. The reaction at the CaO/melt interface considered in this study is shown in Figure 9. First, Ca, which was formed by the reaction shown in Eq. [1], was not only dissolved into the melt but also existed on the surface of the CaO rod. Next, Sb reacted with Ca and O on the surface of the CaO rod, and was removed from the melt through the formation of Sb-Ca-O layer. Since the CaO crucible (CaO: >99.9 vol.%) and the CaO rod (CaO: 98.9, MgO: 0.58, SiO_2: 0.34, Al_2O_3: 0.02, Fe_2O_3: 0.02 vol.%) have similar compositions, it is thought that Sb-Ca-O layer was formed on the surface of the CaO crucible as well.

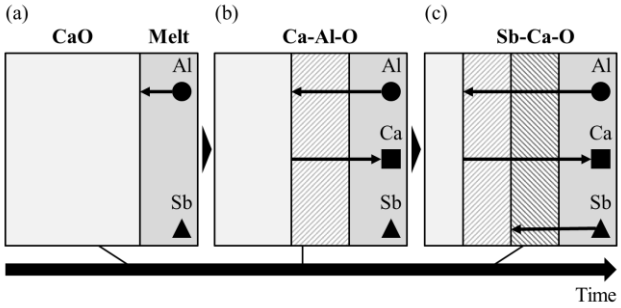

Fig. 9—Schematic diagrams of the reaction at the CaO/melt interface considered in this study. (a) Al in the melt touches the surface of CaO, (b) Ca-Al-O layer is formed and Ca is dissolved in the melt by the reduction of CaO, and (c) it is assumed that Sb-Ca-O layer is formed on the surface of CaO.

C. *Reactions in Melt and Alloy During Solidification*

The formation process of the inclusion in the melt is discussed. The reaction layer consisting of Sb, Ca, and O formed at the CaO/melt interface as shown in the previous section, suggesting that the

complex oxides, which contain Sb, Ca, and O, were formed in the melt at 1600 °C (Figure 10(b-1)). Moreover, the Sb-Ca-O inclusion existed near the grain boundary of the starter of TMS-238+Sb(CaO) as shown in Figure 6, suggesting that Sb, Ca, and O were distributed to the liquid phase (Figure 10(a-2)) or that the complex oxides formed in the melt gathered in the final solidification part (Figure 10(b-2)). Note that the inclusion shown in Figure 6 also presented signs of Zr, which most likely came from the ZrO_2-base mold (66.2 vol pct of ZrO_2, 32.7 vol pct of SiO_2, etc.), that was used to cast the alloy. Various oxides that are components of the crucibles and molds used to fabricate the alloys may be included in these inclusions.

Next, the effect on suppressing Sb segregation at the oxide/substrate interface is discussed. Figure 10(d,e) shows the mechanism behind the improvement of oxidation resistance of Ni-base superalloy containing impurity Sb using CaO. The oxidation resistance of TMS-238+Sb(Al_2O_3) is degraded because Sb diffuses and segregates to the oxide/substrate interface during oxidation tests shown in Figure 4, and this results in the spallation of the oxide layers, as Takata *et al.* revealed[11]. On the other hand, the oxidation resistance of TMS-238+Sb(CaO) improved. This is because the amount of Sb segregation at the oxide/substrate interface decreased as shown in Figure 5. The suppression of Sb segregation at the oxide/substrate interface is likely caused by the removal of Sb from the melt and the fixation of Sb in the alloy, analogous to the previous studies on S[17,18]. In this study, it is likely that the formation of Sb-Ca-O inclusions, which is shown in Figure 6, fixes Sb to the alloy, similar to the effect on fixing impurity S revealed by Tabata *et al.*[17,18]. According to previous research, CaS did not affect the mechanical properties such as creep and fatigue strength[1,6]. Moreover, Sb-Ca-O inclusions found within the alloy do not affect to the spallation of the oxide layers because Sb-Ca-O inclusions were not observed at the oxide/ substrate interface, and its size were smaller than the CaS inclusions. Moreover, in terms of Sb contents, Sb content in TMS-238+Sb(CaO) is slightly higher than that of TMS-238+Sb(Al_2O_3). It is most likely because some of the Sb remained in the melt due to the formation of Sb-Ca-O inclusions inside the melt. In the previous studies[17,18], S contents after CaO crucible melting were also slightly higher than those after Al_2O_3 crucible melting. It is thought that these were due to the formation of CaS inclusions. Therefore, the improvement of oxidation resistance can be attributed to the prevention of spallation of the oxide layers, which is due to the suppression of Sb segregation at the oxide/substrate interface by removal of Sb and fixation of Sb in the alloy by CaO.

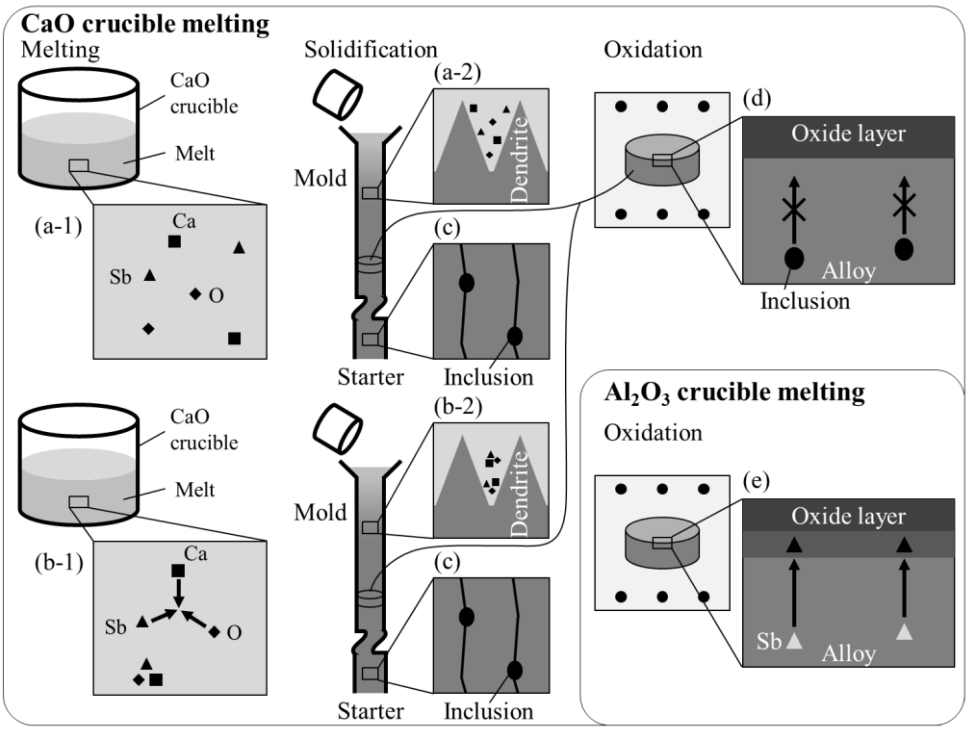

Fig. 10—Schematic diagrams of the reactions in melt and alloy during solidification and oxidation test considered in this study. (a-1) Sb, Ca, and O exist in the melt, (a-2) Sb, Ca, and O are distributed to the liquid phase, (b-1) the complex oxides are formed in the melt, (b-2) the complex oxides gather in the final solidification part, and (c) the inclusions are formed in the final solidification part. During the oxidation test, (d) Sb is fixed in the alloy and (e) Sb segregates at the oxide/substrate interface.

V. CONCLUSIONS

In this study, the following has been made clear through the CaO crucible melting experiments and the CaO rod insertion experiments for Ni-base single crystal superalloy TMS-238 containing impurity Sb.

1. CaO crucible melting improves oxidation resistance of the alloy containing Sb. This is because CaO has the effect on removing Sb from the melt and fixing Sb in the alloy. This leads to the suppression of Sb segregation at the oxide/substrate interface, and the prevention of spallation of the oxide layers.

2. The removal of Sb from the melt occurs by the formation of Sb-Ca-O on the surface of CaO. Sb-Ca-O is formed by the reaction of Sb with O and Ca, which is formed by the reduction of CaO by Al.

3. The fixation of Sb in the alloy occurs by the formation of Sb-Ca-O inclusions in the alloy. Ca

dissolves into the melt by the reaction of CaO and Al, which then reacts with O and Sb to form Sb-Ca-O inclusions.

ACKNOWLEDGMENTS

This research was financially supported by the Council for Science, Technology and Innovation (CSTI), Cross-ministerial Strategic Innovation Program (SIP), "Materials Integration for revolutionary design system of structural materials" (Funding agency: JST) and The Technical Association of Refractories, Japan. The authors are grateful to Dr. Makoto Osawa and Dr. Toshio Osada at NIMS, and Mr. Takahide Horie, a graduate student at Waseda University, for the helpful discussions, Ms. Kyoko Suzuki at NIMS, for the support of the microstructural investigation, and Mr. Lei Tan, a graduate student at Waseda University, for the support of the CaO rod insertion experiment.

CONFLICT OF INTEREST

On behalf of all authors, the corresponding author states that there is no conflict of interest.

REFERENCES

[1] K. Kawagishi, A. Yeh, T. Yokokawa, T. Kobayashi, Y. Koizumi, and H. Harada: *Superalloys 2012*, 2012, pp. 189–95.

[2] P. Caron: *Superalloys 2000*, 2000, pp. 737–46.

[3] L. Liu, J. Meng, J. Liu, M. Zou, H, Zhang, X. Sun, and Y. Zhou: *J. Mater. Sci. Technol. (Shenyang, China)*, 2019, vol. 35, pp. 1917-24.

[4] A. Heckl, S. Neumeier, M. Göken, and R.F. Singer: *J. Mater. Sci. Eng. A.*, 2011, vol. A528, pp. 3435–44.

[5] A.C. Yeh and S. Tin: *Scr. Mater.*, 2004, vol. 52, pp. 519–24.

[6] S. Utada, Y. Joh, M. Osawa, T. Yokokawa, T. Kobayashi, K. Kawagishi, S. Suzuki, and H. Harada: *Superalloys 2016*, 2016, pp. 589–99.

[7] H. Harada, K. Kawagishi, T. Kobayashi, T. Yokokawa, M. Osawa, M. Yuyama, S. Suzuki, Y. Joh, and S. Utada: US Patent, patent number 10689741 (2020.06.23).

[8] R.T. Holt and W. Wallace: *Int. Met. Rev.*, 1976, vol. 21, pp. 1–24.

[9] G.B. Thomas and T.B. Gibbons: *Met. Technol.*, 1979, vol. 6, pp. 95–101.

[10] G.W. Meetham: *Met. Technol.*, 1984, vol. 11, pp. 414–8.

[11] Y. Takata, T. Sugiyama, M. Yuyama, J. Uzuhashi, T. Okubo, H. Harada, S. Suzuki, and K. Kawagishi: *J. Japan Inst. Met. Mater.*, vol. 87, pp. 88-94 (in Japanese).

[12] Y. Nakamura, T. Mukai, M. Kuwabara, and K. Arihara: *Tetsu-to-Hagané*, 1977, Vol. 63, pp.

2246-53 (in Japanese).
[13] H. Wang, T. Zhang, H. Zhu, G. Li, Y. Yan, and J. Wang: *ISIJ Int.*, 2011, Vol. 51, pp. 702–6.
[14] T. Sakai, T. Nakamura, F. Noguchi, and Y. Ueda: *J. Min. Metall. Inst. Jpn.*, 1987, Vol. 103, pp. 587-92 (in Japanese).
[15] Y. Kishimoto, S. Utada, T. Iguchi, Y. Mori, M. Osawa, T. Yokokawa, T. Kobayashi, K. Kawagizhi, S. Suzuki, and H. Harada: *Metall. Mater. Trans. B*, 2020, vol. 51, pp. 293-305.
[16] Y. Kishimoto, T. Kono, T. Horie, T. Yokokawa, M. Osawa, K. Kawagishi, S. Suzuki, and H. Harada: *Metall. Mater. Trans. B*, 2021, vol. 52, pp. 1450-62.
[17] C. Tabata, K. Kawagishi, J. Uzuhashi, T. Ohkubo, K. Hono, T. Yokokawa, H. Harada, and S. Suzuki: *Scr. Mater.*, 2021, vol.194, pp. 113616.
[18] C. Tabata, K. Kawagishi, J. Uzuhashi, T. Ohkubo, T. Yokokawa, H. Harada, and S. Suzuki: *Metall. Mater. Trans. A*, 2022, vol. 53, pp. 2452-8.
[19] B. Gault, M.P. Moody, J.M. Cairney, and S.P. Ringer: *Atom Probe Microscopy*, vol. 160, Springer New York, New York, NY, 2012, pp. 3-7.
[20] R. Izquierdo, E. Sacher, and A, Yelon: *Appl. Surf. Sci.*, 1989, vol. 40, pp. 175-7.
[21] W. K. Liu, W. T. Yuen, and R. A. Stradling: *J. Vac. Sci. Technol., B: Microelectron. Nanometer Struct.*, 1995, vol. 13, pp. 1539.
[22] R.J. Fruehan: *Metall. Trans. B.*, 1978, vol. 9, pp. 287–92.
[23] T. Degawa and T. Ototani: *Tetsu-to-Hagané*, 1987, vol. 73, pp. 1684–90 (in Japanese).

APPENDIX

Interference corrections between Ca and Sb for EPMA on the CaO rods were carried out. In Figure 7, the elemental maps for Sb are the results after interference correction. As shown in Figure A1(a), Sb was detected in the CaO rods, but because the detection wavelengths of Sb (3.4354 Å) and Ca (3.3524 Å) are close, the peak intensity at the detection wavelength of Sb before correction is most likely includes the Ca from the CaO rod. Therefore, the removal of Ca from the peak intensity at the detection wavelength of Sb is needed to know the actual point of Sb existing. In this study, an interference correction method, which subtracts the increment due to the peak intensity of Ca from the peak intensity at the detection wavelength of Sb, was applied. The correction factor *R*, which is the ratio of the average peak intensity at the detection wavelength of Sb, $I^0_{\mathrm{Ca}(3.4354)}$, to the average peak intensity at the detection wavelength of Ca, $I^0_{\mathrm{Ca}(3.3524)}$, was obtained within the range shown in Figure A1(b) for the as-received CaO rod.

$$R = I^0_{\mathrm{Ca}(3.4354)}/I^0_{\mathrm{Ca}(3.3524)} \quad \#[\mathrm{A1}]$$

Multiplying the correction factor *R* by the peak intensity at the detection wavelength of Ca for each sample, $I_{\mathrm{Ca}(3.3524)}$, the increment due to the peak intensity of Ca at the detection wavelength of Sb,

$I_{Ca(3.4354)}$, was obtained.

$$I_{Ca(3.4354)} = R \times I_{Ca(3.3524)} \#[A2]$$

Subtracting the increment due to the peak intensity of Ca at the detection wavelength of Sb, $I_{Ca(3.4354)}$, from the peak intensity at the detection wavelength of Sb, $I_{Ca+Sb(3.4354)}$, the peak intensity of Sb at the detection wavelength of Sb, $I_{Sb(3.4354)}$, was obtained.

$$I_{Sb(3.4354)} = I_{Ca+Sb(3.4354)} - I_{Ca(3.4354)} \#[A3]$$

As shown in Figure 7, the Sb peak disappeared in the as-received CaO rod by the interference correction. Therefore, the increment due to the peak intensity of Ca at the detection wavelength of Sb was removed.

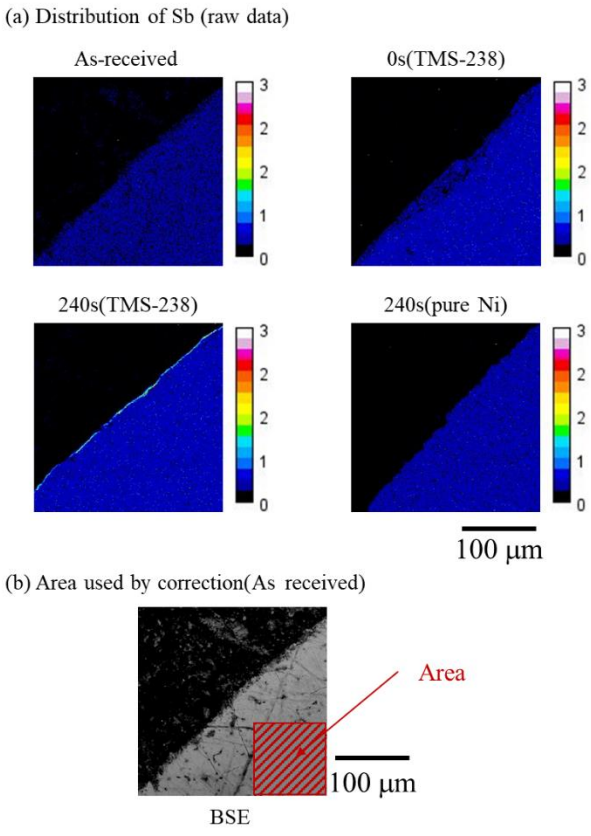

Fig. A1—The interference correction for EPMA of the CaO rods. (a) The distribution of Sb before the interference correction. The unit of the color bars is wt pct. (b) The range used for the interference correction.